Topologically correct synthetic reconstruction of pathogen social behavior found in deep tissue sites

Running title: *Yersinia pseudotuberculosis* replication in microdroplets.

Stacie A. Clark[1,2], Derek Thibault[3], Lauren M. Shull[1,2], Kimberly M. Davis[4], Emily Aunins[1,5], Tim van Opijnen*[3], Ralph R. Isberg*[1,5]

[1]Department of Molecular Biology and Microbiology
[2]Graduate Program in Molecular Microbiology, Tufts University Graduate School of Biomedical Sciences, Boston, MA, USA
[3]Department of Biology, Boston College, Boston, MA, USA
[4] W. Harry Feinstone Department of Molecular Microbiology and Immunology Johns Hopkins Bloomberg School of Public Health, Baltimore, MD, USA
[5]Tufts University School of Medicine, Boston, MA, USA

*Corresponding authors:

E-mails: Ralph.Isberg@tufts.edu (RI); vanopijn@bc.edu (TvO)

Abstract

Within deep tissue sites, extracellular bacterial pathogens often replicate in clusters that are surrounded by immune cells. Disease is modulated by interbacterial interactions as well as bacterial-host cell interactions resulting in microbial growth, phagocytic attack and secretion of host antimicrobial factors. To overcome the limited ability to manipulate these infection sites, we established a system for *Yersinia pseudotuberculosis* (*Yptb)* growth in microfluidics-driven microdroplets that regenerates microbial social behavior in tissues. Chemical generation of nitric oxide (NO) in the absence of immune cells was sufficient to reconstruct microbial social behavior, as witnessed by expression of the NO-inactivating protein Hmp on the extreme periphery of microcolonies, mimicking spatial regulation in tissues. Similarly, activated macrophages that expressed inducible NO synthase (iNOS) drove peripheral expression of Hmp, allowing regeneration of social behavior observed in tissues. These results argue that topologically correct microbial tissue growth and associated social behavior can be reconstructed in culture.

Introduction

A variety of bacterial pathogens colonize and replicate within tissues despite the presence of the host immune system (Carter & Collins, 1974; Cheng et al., 2009; Simonet et al., 1990). Growth in tissue sites involves the formation of distinct foci of replication, which can develop into either abscesses, granulomas, or poorly defined clusters of bacteria (Cheng et al., 2011; Pagan & Ramakrishnan, 2018). Extracellular bacterial pathogens, in particular, can establish a tissue niche and replicate to high numbers. These clusters of bacteria in tissues are often clonal, result in distinct microcolonies, and are surrounded by host innate immune cells.

Yersinia pseudotuberculosis (Yptb) is an enteric pathogen that replicates in the intestinal lumen and regional lymph nodes, with the potential for disseminating via a poorly characterized route into deep tissue sites such as the liver or spleen (Barnes et al., 2006). Once colonized, *Yptb* establishes extracellular foci of replication, resulting in the formation of microcolonies that develop into lesions that are densely populated by immune cells (Simonet et al., 1990). Within the murine spleen, the bacterium sets up a beachhead in which distinct microcolonies are derived from a single seeding bacterium (Davis et al., 2015). Surrounding the bacterial microcolony, which contains between 50-5000 bacteria, are strata of immune cells. In direct contact with the population center are neutrophils, which have cytoskeletal elements that are paralyzed by the abutting bacteria that translocate Type III Secretion System (TTSS) effectors. As a consequence, phagocytosis of the pathogen by surrounding neutrophils is severely disrupted and reactive oxygen species (ROS) production is greatly reduced (Songsungthong et al., 2010). The resulting neutrophil-bacterium interface appears to result in a stable relationship, in which frustrated phagocytes bind, but do not internalize the nearby bacteria. Surrounding this sphere of

neutrophils are macrophages, monocytes, and other immune cells, which appear to be recruited as a response to failure to clear the focus of infection.

The recruitment of neutrophils and macrophages around a cluster of *Yptb* exposes the bacterial population to different microenvironments, depending on the locale within the microcolony occupied by individual bacteria. This drives the phenotypic specialization of different microbial regulatory subpopulations that counter the host attack. Peripheral bacteria that are in direct contact with neutrophils upregulate their T3SS to facilitate disruption of neutrophil function and allow a ring of ineffective immune cells to surround the infection site (Davis et al., 2015). These bacteria are also part of a larger peripheral subpopulation of bacteria that neutralize nitric oxide (NO) gas being produced by the surrounding macrophages, resulting in upregulation of the NO-detoxifying protein, Hmp. The majority of the bacterial peripheral subpopulation that responds to NO is not in direct contact with any host cells, meaning that there is a specialized subpopulation that does not directly interface with host cells, but which responds to humoral anti-microbial factors. Importantly, this peripheral subpopulation participates in social behavior, as its ability to inactivate NO via the Hmp protein protects bacteria in the core of the microcolony from NO stress. In the absence of Hmp protein, the entire microcolony is exposed to NO attack, with the consequence that the microcolony eventually disintegrates and the bacteria are killed in tissues (Davis et al., 2015).

Although live animal models provide valuable insight into the spatial organization of bacterial subpopulations and immune cells in tissue, analysis is currently limited to microscopy of fixed tissue, with little opportunity to study the dynamics of the infection process or perform genetic analysis. Tissue culture models rely on infection of cells within a monolayer, which fail to reproduce the architecture of bacterial microcolonies surrounded by immune cells in host

tissue sites. There has been limited analysis of the dynamics of bacterial growth in tissue, investigation of the spatial relationship between immune cells and the bacteria, or identification of inter-bacterial communication within the growing microbial populations in tissues. To bridge the gap between animal infection models and tissue culture models, we developed a chemical strategy to incorporate the architecture of inflammatory sites in a tissue culture system.

In this report, we develop an *in vitro* system that uses droplet-based microfluidics to generate matrix-embedded *Yptb* microcolonies encompassed by host innate immune cells. Social behavior of *Yptb* could be reproduced in the presence of a chemical NO generator, indicating that production of RNI by host innate immune cells does not require directional targeting of the bacteria by these cells, but rather is a consequence of multi-cell collaboration to generate toxic amounts of RNI. We observed similar results using activated macrophages that express iNOS, mimicking social behavior in tissue. The strength of this approach is that this type of topological analysis of *Yptb*-host cell interaction is unattainable in murine and tissue culture models of infection, allowing for development of high throughput screens not accessible using current culture systems.

Results

Droplet gels support clonal growth of *Yersinia pseudotuberculosis* microcolonies.

Yptb microcolonies in the murine spleen are derived from single isolated bacteria that replicate as extracellular clusters and become surrounded by innate immune cells (Davis et al., 2015; Simonet et al., 1990). In order to accurately model the growth of *Yptb* in deep tissue sites, a single bacterium needs to be isolated and grown into a microcolony in a matrix that supports this 3-dimensional (3D) topology. To encase single bacterial cells in matrix, we utilized droplet-

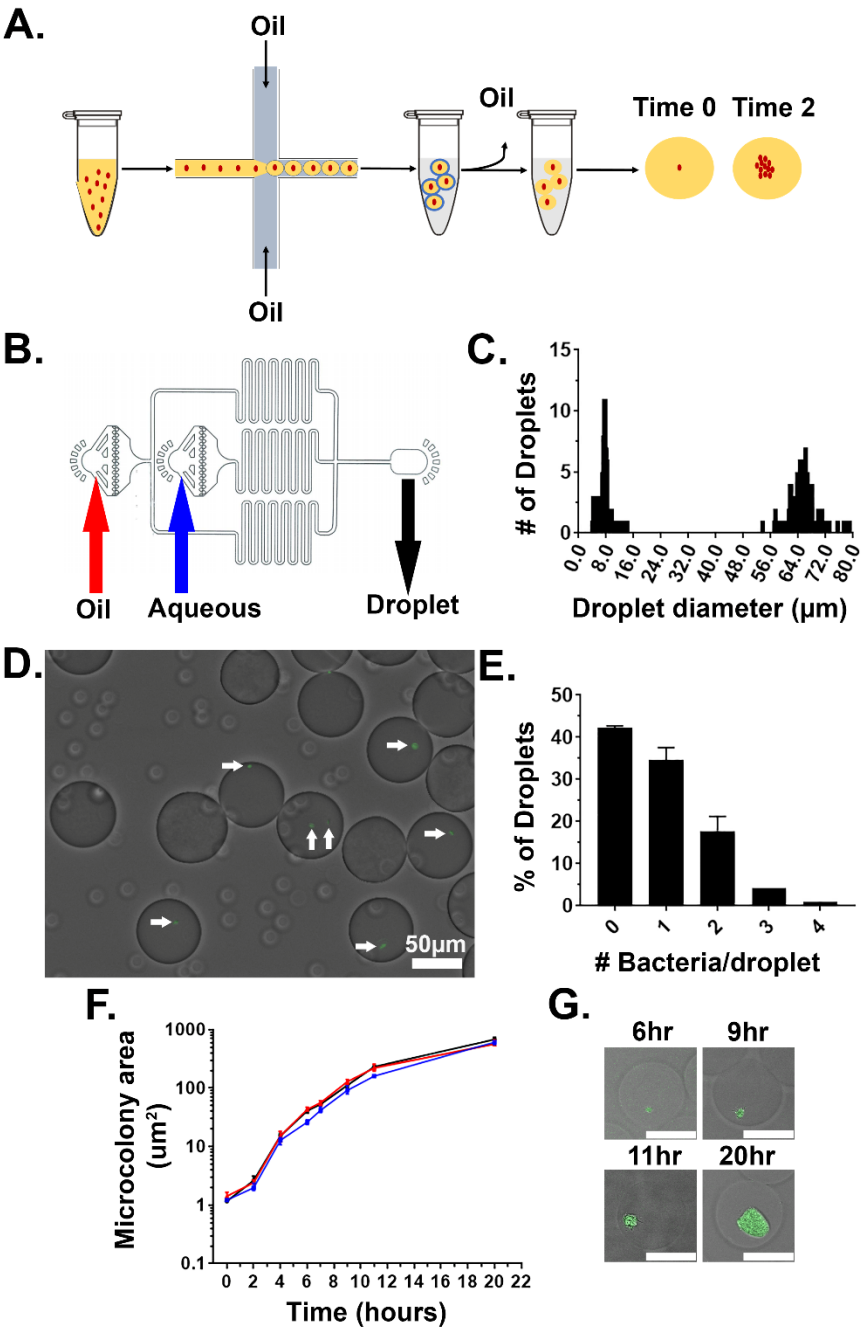

Figure 1. Droplet gels support clonal growth of *Yersinia pseudotuberculosis.* A. *Y. pseudotuberculosis* was added to molten agarose/HyStem®-C Hydrogel and introduced into a microfluidics device, allowing encapsulation within oil-coated droplets (Materials and Methods). Oil was removed from the droplets and bacteria were cultured *in situ* within the droplets (Thibault et al., 2019). B. Design of the microfluidics device. Noted are oil and aqueous (molten gel/bacteria mixture) phase inlets (red and blue arrows, respectively). Droplets were collected into a tube at the droplet output (black arrow) (Thibault et al., 2019). C. Distribution of droplet sizes prior to oil removal. Droplet size was determined by capturing images from phase contrast microscopy followed by image processing (Materials and Methods). D, E. Droplets largely contain one or two bacterial cells immediately after encapsulation. D. Image of droplets containing *Y. pseudotuberculosis gfp*$^{+}$. E. Presence of bacteria was scored immediately after encapsulation by phase contrast and fluorescence microscopy, scoring for GFP. F. *Y. pseudotuberculosis* grows within colonies in droplets. Droplets containing encapsulated *Y. pseudotuberculosis* were cultured at 26°C, and microcolonies were visualized at indicated timepoints by phase contrast and fluorescence microscopy. Microcolony areas were determined by image analysis (Materials and Methods). Each timepoint is median +/- 95% confidence interval

(CI) of 3 biological replicates of 50 microcolonies. G. Representative images of microcolonies from (F) at the noted times visualized by phase contrast and fluorescence microscopy. Scale bar: 50μm.

based microfluidics, which is commonly used for isolating single mammalian cells (Koster et al., 2008; Macosko et al., 2015; Mazutis et al., 2013).

Yptb was added to a matrix consisting of molten 1% ultra-low melt agarose containing 25% HyStem®-C Hydrogel. HyStem®-C Hydrogel has thiol-modified hyaluronan and gelatin, allowing on-demand polymerization of these two components controlled by the addition of a thiol-reactive crosslinker (Fig. 1A). The biomatrix was included in the droplet mixture to add components that allow multivalent adhesion sites for attachment of mammalian immune cells (Cha et al., 2017; Giancotti & Ruoslahti, 1999). The mixture was then placed in a syringe pump and under constant flow injected into a fabricated two-inlet microfluidics device, with oil introduced into the other inlet, allowing encapsulation of the bacteria in a droplet matrix surrounded by oil (Fig. 1B; Materials and Methods). At a final concentration of $5x10^6$ bacteria/ml, the majority of droplets contained a single bacterium, as predicted by the Poisson distribution (Fig. 1D and 1E) (Mazutis et al., 2013; Thibault et al., 2019). Notably, there were two groups of droplets that were collected in the output (Fig. 1C). The large droplets contained bacteria and were approximately 65 μm in diameter (~144 pl), while the small, satellite droplets were about 8 μm in diameter (Fig. 1C and 1D). After droplet generation, HyStem®-C Hydrogel was crosslinked within the agarose using Extralink®, a thiol-reactive crosslinker, at room temperature and oil was removed from the droplets (Materials and Methods). During oil removal, the population of small droplets was lost, and only the larger droplets remained.

In tissue, *Yptb* microcolonies form clusters (Simonet et al., 1990). We wanted to confirm that *Yptb* grows as a cluster inside the agarose/ HyStem®-C Hydrogel droplets. To this end *Yptb* expressing GFP (Ptet*::gfp,* expressed from pACYC184) was encapsulated in droplets, oil was removed, and the droplets were incubated at 26 ºC in 2xYT broth with rotation. Microcolony

136 growth was determined by identifying a threshold that defines edges of microcolonies in the GFP
137 channel and determining the number of pixels in the region of interest (ROI). The data were then
138 converted to metric scale using a stage micrometer and displayed as μm^2. The area of the
139 microcolony increased over time with roughly logarithmic kinetics over a 10-hour period,
140 indicating that the agarose/ HyStem®-C Hydrogel droplets support efficient *Yptb* microcolony
141 formation (Fig. 1F). The replicating bacteria also grew in clusters, with similar appearance to *Y.*
142 *enterocolitica* grown in collagen gels (Fig. 1G) (Freund et al., 2008). Altogether, these results
143 show that agarose/ HyStem®-C Hydrogel droplets support microcolony formation of *Yptb*,
144 mimicking growth and topological constraints observed in tissue.
145
146 **Droplet-generated *Yersinia pseudotuberculosis* microcolonies require Hmp to maintain**
147 **growth in the presence of NO**
148 Upon sensing of microbes, inducible NO synthase (iNOS) is synthesized by immune cells
149 to produce gaseous NO as an important line of host defense (Bogdan, 2001). NO has
150 antimicrobial properties and can react with ROS to produce additional toxic reactive nitrogen
151 intermediates (RNI). The bacterial protein, Hmp, detoxifies NO by converting it to nitrate (NO_3)
152 which is innocuous and can be used as an electron acceptor by the pathogen (R K Poole et al.,
153 1996; R. K. Poole & Hughes, 2000; Robinson & Brynildsen, 2013). During growth in the murine
154 spleen, bacteria located on the periphery of microcolonies express *hmp*, and loss of Hmp
155 attenuates *Yptb* disease (Davis et al., 2015). To evaluate if Hmp is also required during growth in
156 droplet microcolonies in the presence of NO, droplet microcolonies and broth cultured bacteria
157 were comparatively evaluated for NO sensitivity. *Yptb* WT and Δ*hmp gfp*+ were encapsulated in
158 droplets, cultured *in situ* for 7 hours, and exposed to varying concentrations of the NO donor

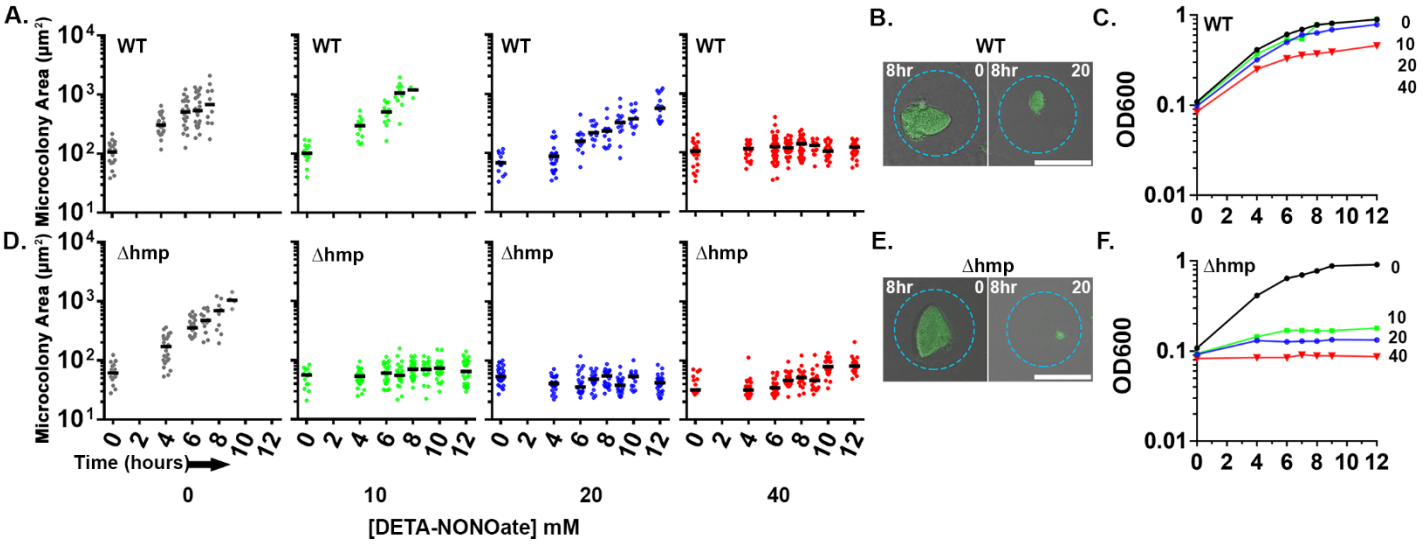

Figure 2. Droplet-generated *Yersinia pseudotuberculosis* microcolonies require Hmp to maintain growth in presence of NO. Indicated *Y. pseudotuberculosis* strains were cultured in 2xYT with rotation at 26 °C for 7 hours prior to DETA-NONOate exposure. At the indicated timepoints, an aliquot of droplets was fixed and visualized by fluorescence microscopy. (A, D). Microcolony area determined from captured images followed by image analysis (Materials and Methods). Each point represents a single droplet with median noted. (B, E). Representative WT (B) and Δ*hmp* (E) microcolonies after 8 hours of treatment with and without DETA-NONOate. Scale bar: 50μm. (C, F). Overnight broth cultures of *Y. pseudotuberculosis* were diluted 1:10 in 2xYT broth prior to addition of DETA-NONOate. At indicated timepoints, culture density was determined (Materials and Methods).

DETA-NONOate. Microcolony area was measured over time through a single plane. In parallel, the two strains were grown in broth culture. The growth of the WT and Δ*hmp* microcolonies was similar in the droplets in the absence of DETA-NONOate (Fig. 2A and 2D). The microcolonies derived from WT were relatively resilient to NO insult, with complete blockage of growth only observed at extreme concentrations (40mM DETA-NONOate) (Fig. 2A). In contrast, the Δ*hmp* strain was blocked from replicating in droplets at all concentrations of DETA-NONOate tested, indicating that Hmp is essential for growth under these conditions (Fig. 2D). Although 8 hours of 20mM DETA-NONOate exposure showed some interference with replication in microdroplets, the WT microcolonies were clearly larger than Δ*hmp* mutant microcolonies (Fig. 2B and 2E). Similar results were observed during growth in broth culture (Fig 2C and F). The Δ*hmp* mutant strain was sensitive to all doses of DETA-NONOate in broth culture, while growth of the WT strain was relatively unaffected at lower doses (Fig. 2C and 2F). At the highest dose used (40 mM), the microdroplet-encased WT colonies showed enhanced sensitivity relative to bacteria grown in broth (Figs. 2A and 2C). Nevertheless, these results indicate that Hmp is required to maintain optimum growth of microcolonies in the presence of NO.

Topological constraints drive non-uniform expression of *hmp*.

During infection by *Yptb*, subpopulations of bacteria within microcolonies respond to distinct microenvironments (Davis et al., 2015). Peripheral bacteria upregulate Hmp to detoxify products of iNOS generated by immune cells, while interior bacteria are protected from RNI and show no such upregulation. The droplet microcolonies are morphologically similar to microcolonies during infection, so we predicted that *hmp* would also be expressed peripherally in response to DETA-NONOate. To probe for non-uniform expression in response to DETA-

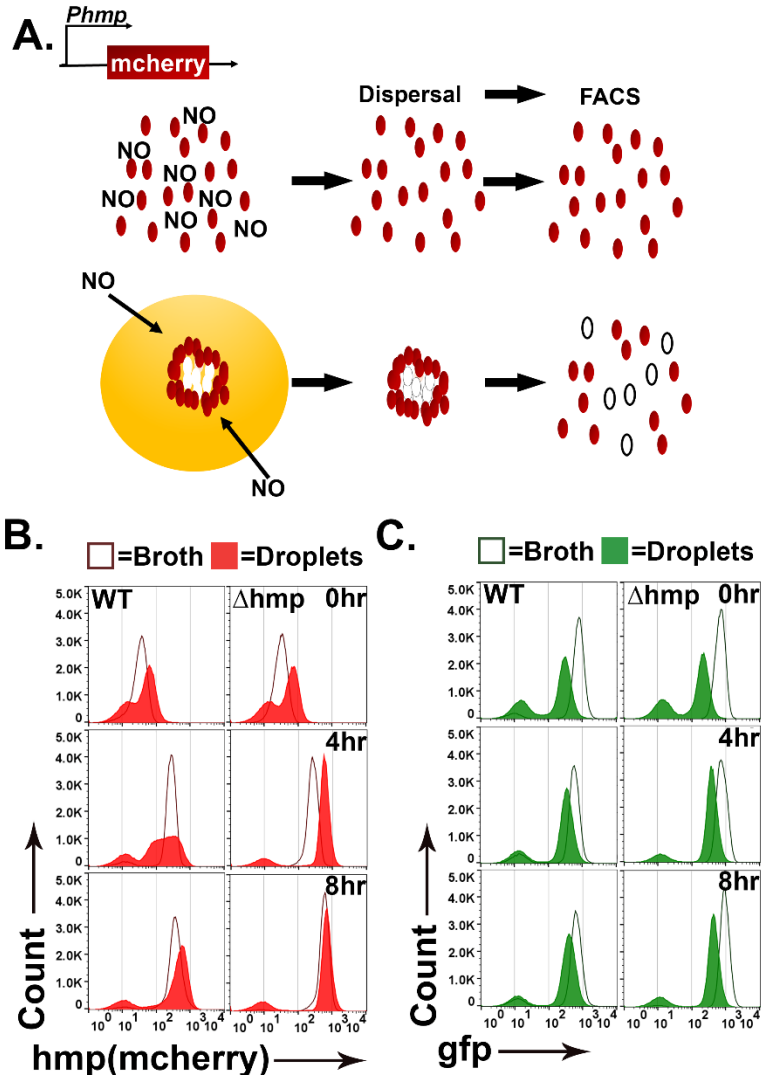

Figure 3. Topological constraints drive non-uniform expression of *hmp*. (A). Model of the predicted outcome for the nitric oxide (NO) response of *Y. pseudotuberculosis* grown in broth versus droplet culture (Davis et al., 2015). Red: bacteria showing high expression of P_{hmp}-*mCherry* reporter. White: bacteria showing undetectable mCherry fluorescence. (B, C). *Y. pseudotuberculosis* grown in droplet microcolonies show altered response to NO. Noted bacterial strains harboring *gfp*$^+$ P_{hmp}-*mcherry* plasmids were grown in either broth (open histograms) or droplets (filled histograms) in the presence of NO donor for the noted times. Droplet microcolonies were dispersed at noted times and analyzed by flow cytometry (Materials and Methods). B. Flow analysis of mCherry channel. C. Analysis of GFP channel.

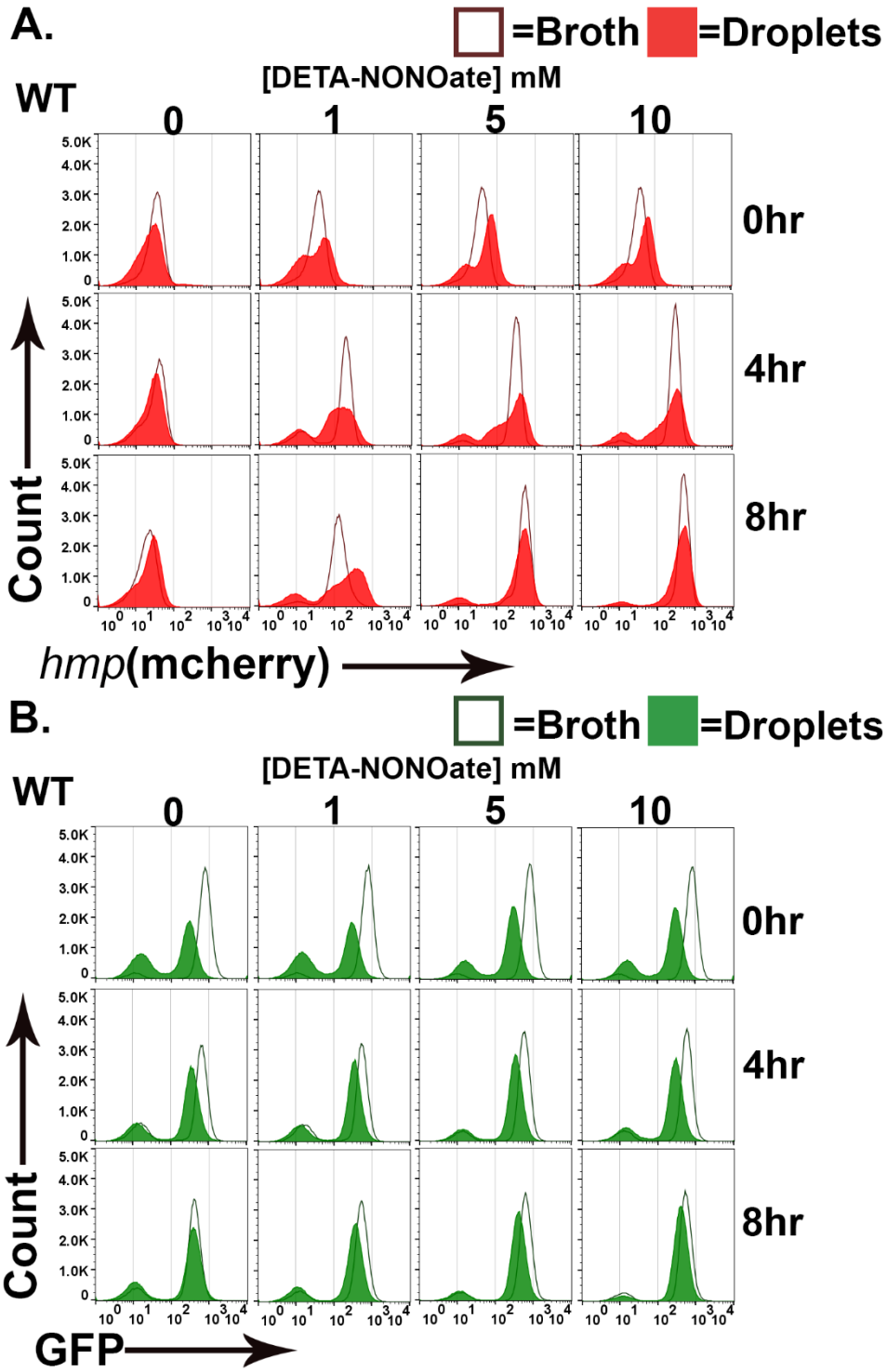

Figure S1. Topological constraints drive non-uniform expression of *hmp*. (A-D). *Y. pseudotuberculosis* grown in droplet microcolonies show altered response to NO. Noted bacterial strains harboring *gfp*$^{+}$ P_{hmp}-*mcherry* plasmids were grown in either broth (open histograms) or droplets (filled histograms) in the presence of NO donor for the noted times. Droplet microcolonies were dispersed at noted times and analyzed by flow cytometry (Materials and Methods). A. Flow analysis of mCherry channel from WT. B. Analysis of GFP channel from WT. C. Flow analysis of mCherry channel from Δhmp. C. Analysis of GFP channel from *Δhmp*.

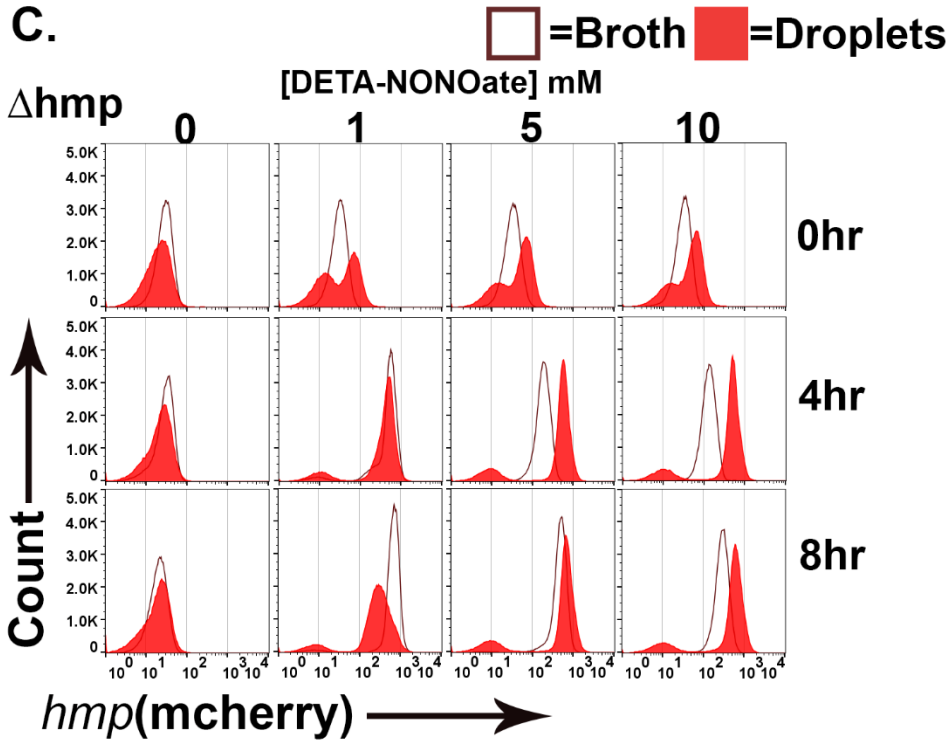

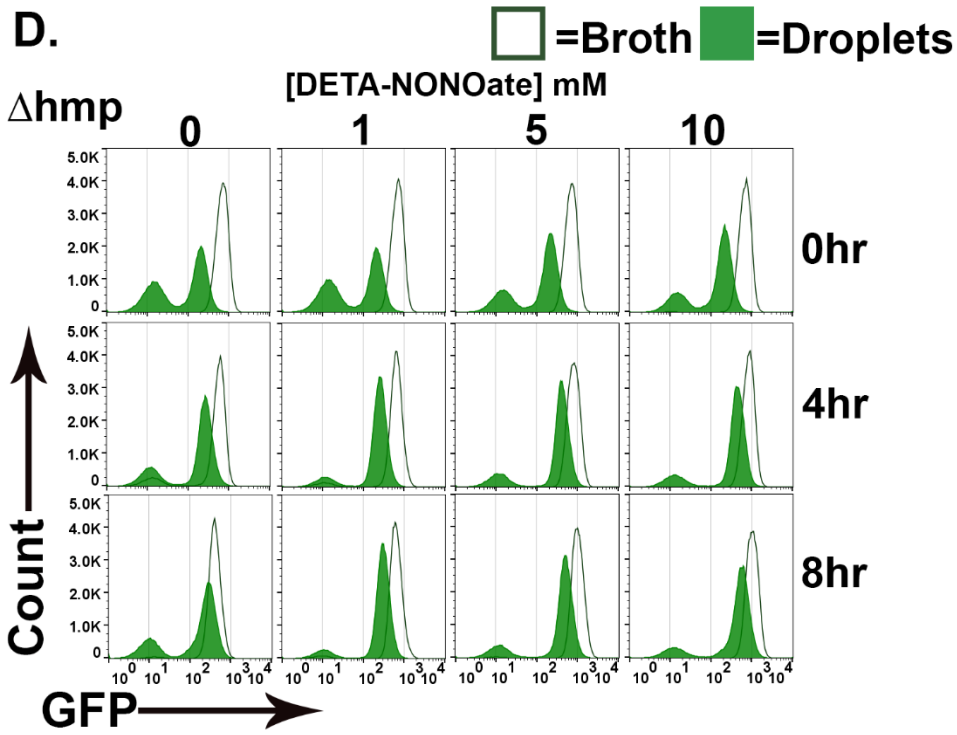

NONOate, we compared the fluorescence of WT and Δ*hmp gfp*+ bacteria harboring a plasmid with the promoter of *hmp* driving expression of mCherry *(Phmp::mcherry*) after exposure to DETA-NONOate using flow cytometry. *Phmp::mcherry* expression should be uniform in broth cultures of WT *Yptb*, while *hmp* should exhibit nonuniform expression in droplets if microcolony structure drives spatial regulation of *hmp* expression (Fig. 3A: left).

To compare *Yptb* grown in droplet microcolonies to bacteria in broth cultures, a protocol was developed to disperse droplet microcolonies into single cells (Fig. 3A; Materials and Methods), to allow flow cytometry analysis of the constitutive *gfp* and *Phmp*::*mcherry* reporters. The WT and Δ*hmp* strains harboring gfp^+ *Phmp::mcherry* were cultured in either droplet microcolonies or broth and exposed to 0,1, 2.5, 5, and 10 mM of DETA-NONOate for 0, 4 and 8 hours (Fig. 3B and C, Fig. S1**)** followed by flow cytometry analysis. In broth grown cultures, WT and Δ*hmp* strains harboring *Phmp::mcherry* showed fluorescence intensity increases after NONOate exposure, with a single population of both *gfp* and *Phmp* high expressers and small populations of nonexpressers in all cases (Fig. 3B: dark-lined, open histograms). In contrast, starting at 4 hours post-exposure of DETA-NONOate to WT microcolonies growing in droplets, there was a broad distribution of *Phmp::mcherry* fluorescence compared to either broth culture or to the *gfp* fluorescence (Fig. 3B red-shaded profile: 4hr and S1A). Continued exposure to NONOate for 8 hours partially dissipated this broad peak, as the distribution of mCherry became more uniform and intense, although the fluorescence profile of the WT strain in microcolonies was clearly broader than when grown in broth culture (Fig. 3B: 8hr and S1A). These results are consistent with microcolony structure driving heterogeneous expression of *Phmp*::*cherry* in response to an RNI generator, with prolonged exposure decreasing heterogeneous firing of the promoter.

The heterogeneous *mcherry* reporter fluorescence in WT was dependent on the *hmp* promoter, as GFP expression driven by the unrepressed Tet promoter was uniform in bacteria that originate from broth culture and droplet microcolonies (Fig. 3C and S1B). Similar to the observations with *mcherry* there was a small population representing approximately 5% of the bacteria that failed to fire *gfp* perhaps due to the dispersal and fixation procedure. These results argue that microcolony topology is a critical factor that drives heterogeneity observed in bacterial subpopulations in response to different microenvironments.

The heterogenous distribution of *Phmp*::*mcherry* fluorescence was dependent on the presence of the Hmp protein. The introduction of the Δ*hmp* mutation resulted in a distribution of *hmp*::*mcherry* fluorescence intensity from droplet microcolonies that was similar to that observed in broth cultures, although there was more rapid firing of the reporter than in broth, with maximal fluorescence already established after 4 hours exposure to DETA-NONOate (Fig. 3B: right and S1C). Therefore, the entire microcolony has the potential to respond to RNI in the absence of Hmp, consistent with the Hmp protein acting to lower the amount of inducing RNI in a subpopulation of bacteria.

Spatial regulation of *hmp* expression in tissues can be reproduced in droplet culture.

We hypothesized that the heterogenous distribution of *Phmp::mcherry* fluorescence of WT *Yptb* as seen by flow cytometry analysis is indicative of spatial regulation of the promoter. To determine if the spatial regulation of *Phmp* observed in tissue can be reproduced in droplet culture, WT and *Δhmp* strains carrying the *gfp*$^{+}$ and *Phmp::mcherry* reporters were encapsulated in droplets, grown into microcolonies, and exposed to DETA-NONOate for 4 hours (Fig. 4A). WT microcolonies showed peripheral expression of *hmp*, while microcolonies lacking Hmp

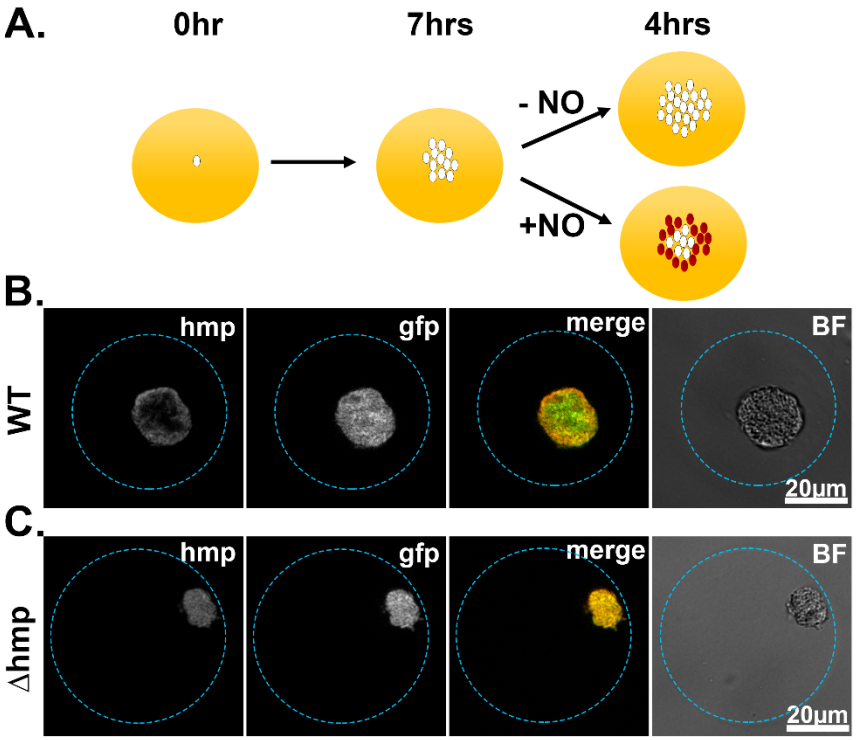

Figure 4. Spatial regulation of *hmp* expression in tissues can be reproduced in droplet culture. (A). Experimental overview. Droplets seeded with *Y. pseudotuberculosis* harboring fluorescence reporters were incubated for 7 hours at 26 °C and varying concentrations of DETA-NONOate were added to the cultures for 4 hours at 37 °C, 5% CO_2. After 4 hours, the droplets were fixed and visualized using brightfield and fluorescence microscopy. (B, C). Representative WT and Δ*hmp* microcolonies after 4 hours of treatment with 1mM DETA-NONOate.

show uniform expression of the *hmp* reporter (Fig. 4B and 4C, respectively). Peripheral expression was dependent upon the NO-driven signal, as the constitutive GFP signal was uniform throughout the microcolonies (Fig. 4B).

To quantitatively analyze spatial regulation of *hmp*, an automated script was developed from images captured using a 63X lens (Fig. 5A). The script defines the periphery of microcolony and sets a mask to determine the region of interest (ROI), allowing a user-defined width extending into the microcolony (12 pixel-radius structuring elements used throughout study) and a point of lowest intensity (PLI, 5 pixel-radius structuring element used here) identified in each ROI (determinants displayed in Fig. 5B). The fluorescence at the periphery is calculated as a ratio of the average pixel intensity of the mCherry channel divided by the average pixel intensity of the GFP channel in the periphery. The fluorescence at the PLI is also calculated this way and the periphery versus PLI ratio is determined. A ratio greater than 1 indicates preferential peripheral expression of *Phmp::mcherry.*

There was a significant increase in the periphery vs. PLI ratio in WT microcolonies in response to DETA-NONOate after 4 hour exposure at concentrations of 1 or 2.5 mM, indicating peripheral expression of *hmp::mcherry* (Fig. 6A,left; $P < 0.0001$). Peripheral expression in the presence vs. absence of RNI stress was independent of colony size, as there was no difference in microcolony area after DETA-NONOate exposure in WT microcolonies (Fig. 6B: left). Microcolonies lacking Hmp, in contrast, had uniform expression of the *hmp* reporter indicated by a ratio ~1 (Fig. 6A: right). Interestingly, the periphery vs PLI ratio in microcolonies lacking Hmp significantly decreased in the presence of DETA-NONOate ($P<0.0001$). This indicates that RNI likely accumulate in the center of microcolonies in the absence of Hmp, a phenomenon also observed in tissue (Davis et al., 2015). Microcolonies lacking Hmp were significantly smaller

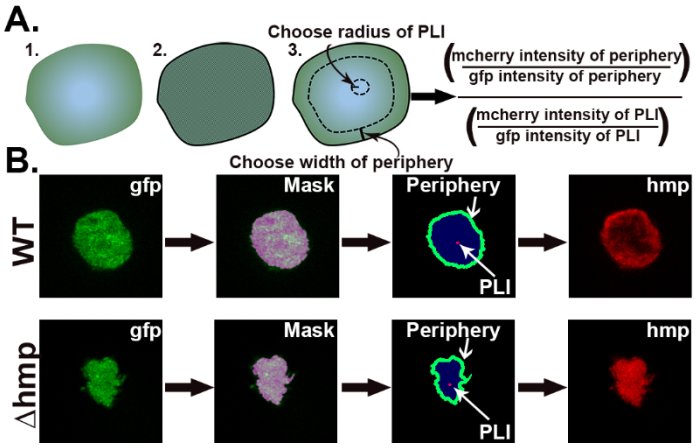

Figure 5. Strategy for quantification of *hmp* expression localized on periphery of microcolonies. A. Design of script that allows the identification of regions of interest (ROIs) for the purpose of determining the average fluorescence intensities and normalization strategies within the ROIs. Script defines periphery of microcolony and sets mask, allowing a user-defined width extending into the microcolony along with a point of lowest intensity (PLI) which is determined based on the mCherry signal for each microcolony. The fluorescence at the periphery is calculated as a ratio of the average pixel intensity of the mcherry channel in periphery divided by the average pixel intensity of the GFP channel in the periphery, allowing normalization for bacterial expression. The fluorescence for the defined PLI is also calculated in the same fashion, and the periphery verses PLI ratio is determined (Supplemental Data). B. Example of identification of periphery, mask generation and definition of peripheral ROI. The GFP channel defines the periphery, allowing mask to be set. Within the mask, the periphery is defined as extending 12 pixels into the microcolony. The PLI within the mask is defined as the area of 5-pixel radius with the lowest intensity in the mCherry channel.

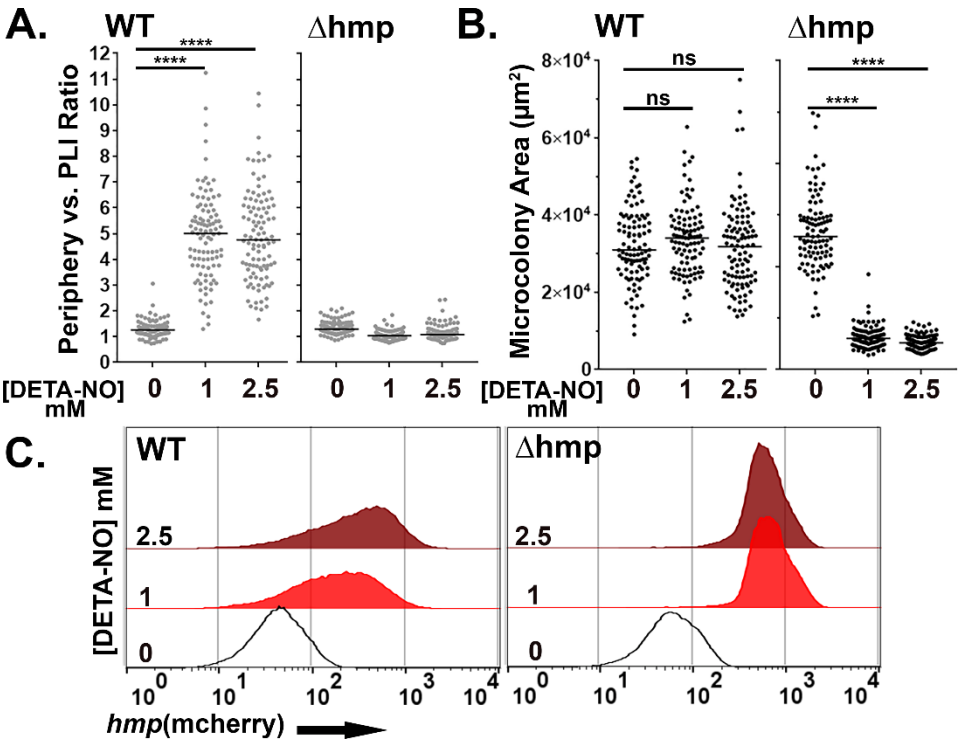

Figure 6. Hmp activity is required for peripheral expression of *hmp* in response to NO. (A-C). The presence of Hmp activity is required for *Y. pseudotuberculosis* to have enhanced expression of P_{hmp} in microcolonies exposed to NO. A. Periphery versus PLI ratio for microcolonies as a function of DETA-NONOate concentration in microcolonies from noted bacterial strains. B. Microcolony area (pixels^2) for WT and Δ*hmp* microcolonies at different concentrations of DETA-NONOate. Black circles: 100 individual microcolonies measured for each condition. Lines indicate the medians. (C). Flow cytometric analysis of dispersed microcolonies. Droplets were dispersed into single cells after 4 hours of DETA-NONOate treatment at noted concentrations and subjected to flow cytometry (Materials and Methods). Bacteria were gated for GFP$^+$ and analyzed for mCherry signal. Statistics: Mann-Whitney test, ****p<0.0001, ns: not significant.

after DETA-NONOate exposure, further showing detoxification by Hmp is required for the growth of a microcolony (Fig. 6B: right, $P<0.0001$).

Flow cytometry analysis of WT *Yptb* originating from droplet microcolonies exposed to these low DETA-NONOate levels revealed heterogenous expression when compared to bacteria that were not exposed to DETA-NONOate (Fig. 6C: left). This argues that the broad distribution of *mcherry* fluorescence intensity is a consequence of spatially regulated *Phmp* firing (Fig. 6A). In contrast, *Yptb Δhmp* microcolonies challenged with DETA-NONOate for 4 hours revealed a tight distribution of *mcherry* fluorescence, indicating penetration of RNI through the entire microcolony (Fig. 6C: right). Therefore, the contour of fluorescence expression from a reporter construct was diagnostic of heterogeneous expression patterns.

Activated BMDMs drive peripheral expression of *hmp* in droplet microcolonies.

NO gas is produced by $iNOS^+$ cells around the periphery of a neutrophil encased *Yptb* microcolony (Fig. 7A). The $iNOS^+$ cells recruited to the inflammatory site consist of monocytes and macrophages ($CD68^+$) cells and are physically separated from the bacterial microcolony (Fig. 7A: right) (Davis et al., 2015). When seeding is initiated, or microcolonies are small, there are very few $iNOS^+$ cells near the site of bacterial replication (Fig. 7A; Seeding Event, Neutrophil Recruitment). Once the colony is completely surrounded by neutrophils, $iNOS^+$ cells are apparent, forming a sphere about recruited neutrophils. Recruitment of $iNOS^+$ cells to a site of bacterial replication as a second step in bacterial restriction is consistent with work done in other pathogens (MacMicking et al., 1997; Murray & Nathan, 1999; Shiloh et al., 1999; Shiloh & Nathan, 2000; Vazquez-Torres et al., 2000). The 65 μm droplets, with bone marrow-derived macrophages (BMDMs) associated with their surface, are predicted to allow extremely good

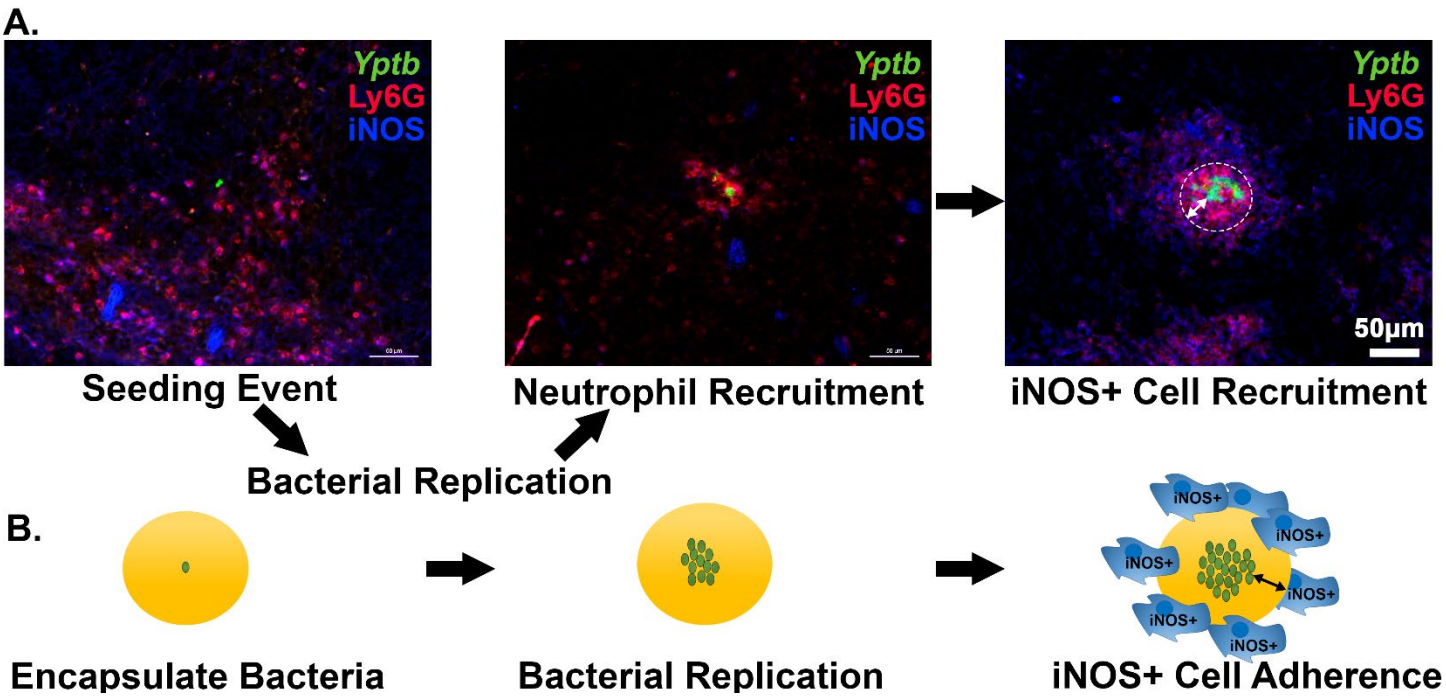

Figure 7. Recruitment of iNOS$^+$ cells is associated with the maturation of *Yersinia pseudotuberculosis* microcolonies in tissue. A. C57BL/6 mice were inoculated intravenously (i.v.) with 10^3 WT *gfp*+ bacteria, and spleens were harvested 3 days post-inoculation (PI). Spleen tissue was probed with α-Ly6G and α-iNOS and visualized by fluorescence microscopy. Neutrophils (α-Ly6G$^+$; red) surround a cluster of *Y. pseudotuberculosis* (green). Surrounding the sphere of bacteria that is encased by neutrophils (white circle) is a layer of iNOS+ cells. White arrows: The distance between *Y. pseudotuberculosis* and the iNOS+ cell layer (not to scale). B. Model for droplet microcolonies. Bacteria are grown *in situ* within the droplets prior to challenge with iNOS$^+$ cells to mimic *Y. pseudotuberculosis* microcolony structure in tissue. Black arrows note there is space between iNOS+ cells and cluster of bacteria.

mimicking of action-at-a-distance by iNOS$^+$ cells, as the microcolonies in the engineered system are situated at similar distances relative to the droplet surface (Fig. 7A, iNOS$^+$ Cell Recruitment). To recapitulate tissue dynamics, therefore, BMDMs were activated to produce iNOS$^+$ and added to droplets containing pregrown microcolonies (Fig. 7B). The agarose/ HyStem®-C Hydrogel droplet served as the buffer zone between the bacterial microcolony and the iNOS$^+$ cell layer (Fig. 7B). Pregrowth of the microcolony prior to exposure to BMDMs is envisioned to recapitulate the kinetics observed from histology of spleen tissues (Fig. 7A).

LPS and IFNγ were incubated with BMDM to activate iNOS, prior to adding the cells for 4 hours to droplets harboring microcolonies previously grown for 7 hours (Fig. 8A and 8B) (Frawley et al., 2018; Green et al., 1994; Mosser & Gonçalves, 2015). Efficient expression of iNOS was dependent on LPS/IFNγ treatment, based on immunofluorescence probing with anti-iNOS (Fig. 8B, left panel). Using this system, WT microcolonies encapsulated in droplets incubated with activated BMDMs exhibited spatially regulated expression of the *Phmp::mcherry* reporter that appeared to exactly mimic the behavior of bacteria growing in tissue (compare Fig. 8C and 8D). As observed in tissues (Davis et al., 2015), this spatial regulation was lost in the Δ*hmp* strain in response to the addition of the activated BMDMs (Fig. 8E). Consistent with the activated BMDMs producing anti-microbial levels of iNOS, growth of the *Δhmp* strain was severely inhibited by the addition of BMDMs at a distance, dependent on the addition of LPS/IFNγ and the presence of active iNOS (Fig. 8F; $p < 0.0001$). Surprisingly, WT microcolonies were significantly larger in the presence of activated BMDMs, partially dependent on the presence of iNOS (Fig. 8F). This is consistent with activated macrophages providing soluble growth-promoting substances at a distance, including either NO_3^- or oxidized cofactors as a consequence of Hmp activity.

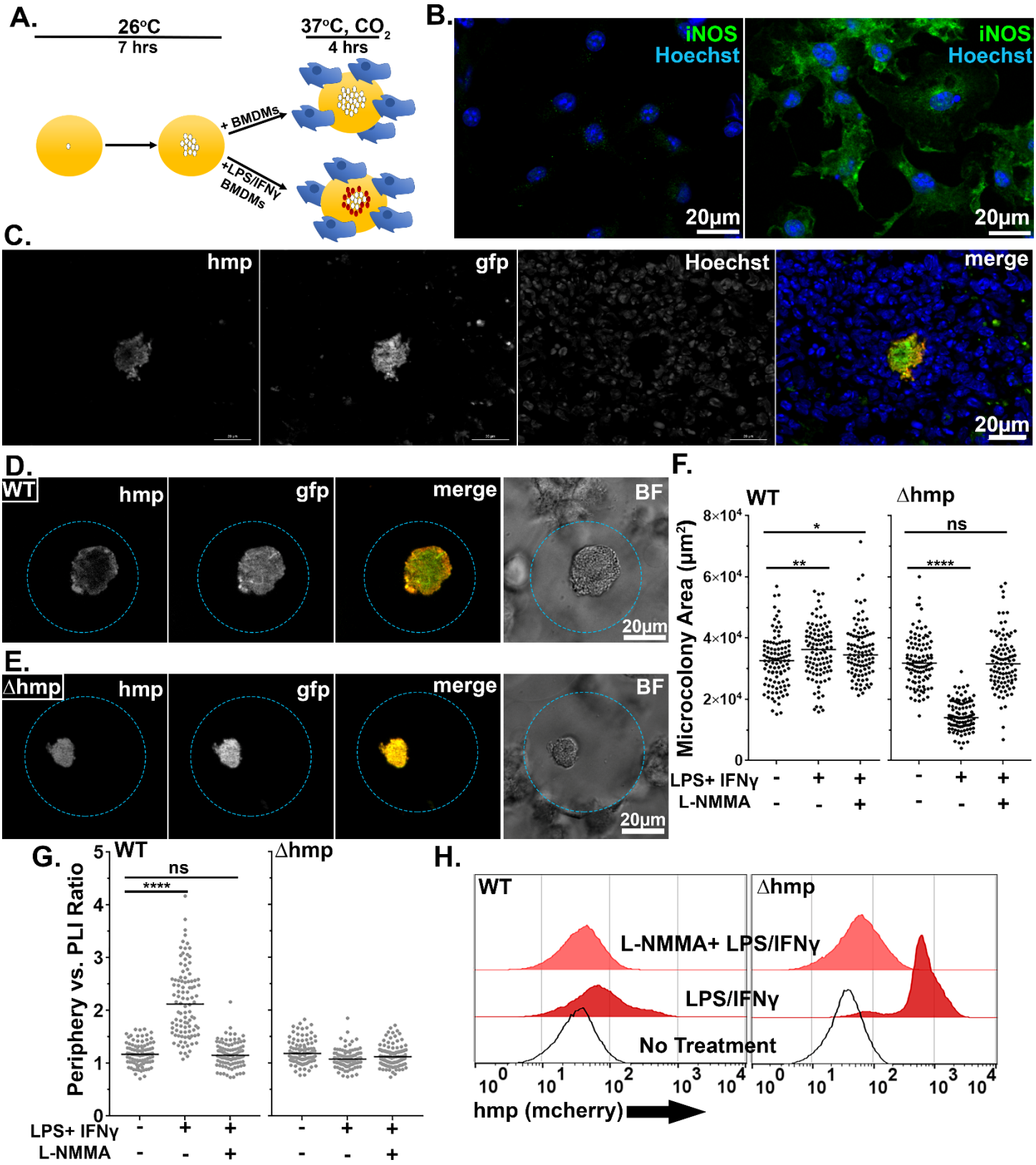

Figure 8. Activated BMDMs drive peripheral expression of *hmp* in droplet microcolonies, mimicking tissue spatial regulation. A. Experimental overview. Droplets containing *Y. pseudotuberculosis* were grown for 7 hours at 26 °C prior to incubation with BMDMs for 4 hours at 37 °C, CO_2. The fixed microcolonies were visualized using brightfield and fluorescence microscopy and subjected to image analysis (Materials and

Methods). B. Resting BMDMs (left) and LPS/IFNγ-primed BMDMs (right) were fixed, probed with α-iNOS and visualized by fluorescence microscopy. (C). C57BL/6 mice were inoculated intravenously (i.v.) with 10^3 WT *gfp+* P_{hmp}*-mcherry* bacteria, and spleens were harvested 3 days post-inoculation (PI) for fluorescence microscopy. A representative microcolony from tissue is shown. (D, E). Representative WT (D) and Δ*hmp* (E) microcolonies incubated with LPS/IFNγ-primed BMDMs. (F). Microcolony area in presence of BMDMs, incubated as noted. (G) Periphery verses PLI ratios for microcolonies incubated with BMDMs treated as noted. Black circles: 100 individual microcolonies from each condition. Line indicates median. (H). Flow cytometry of dispersed microcolonies after 4 hours of incubation with BMDMs. Dispersed bacteria were gated for GFP^+ and mCherry fluorescence was determined (Materials and Methods). Statistics: Mann-Whitney test, ****p<0.0001, ***p<0.0005, **p<0.005, *p<0.05, ns: not significant.

297 To show that peripheral expression of *hmp* was dependent upon RNI, the NOS inhibitor,
298 L-NMMA, was introduced into this system (Fig. 8F, G). BMDMs were incubated in the presence
299 or absence of 2mM L-NMMA prior to challenging droplet microcolonies, and expression of the
300 *Phmp::mcherry* reporter was analyzed by microscopy (Frawley et al., 2018). In response to
301 LPS/IFNγ-primed BMDMs, there was a large increase in peripheral expression of the
302 *Phmp::mcherry* reporter relative to the addition of BMDMs in the absence of activation (Fig.
303 8G; $p<0.0001$). Peripheral expression of the mCherry reporter was lost in WT microcolonies
304 when iNOS was inhibited by NMMA, with the resulting distribution being indistinguishable
305 from BMDMs in the absence of activation (Fig. 8G). As expected, there was no spatial
306 regulation of *Phmp::mcherry* in the strain lacking *hmp* activity, and the presence of NMMA had
307 no effect (Fig. 8G). These results indicate that peripheral expression of *Phmp::mcherry* is
308 dependent on the presence of intact Hmp protein and in response to RNI generated by iNOS
309 activity.
310 To demonstrate that there was heterogeneous *hmp* expression in WT microcolonies on a
311 population level, WT and Δ*hmp* microcolonies challenged with unprimed, LPS/IFNγ-primed, or
312 L-NMMA treated-LPS/IFNγ-primed BMDMs were dispersed and analyzed by FACS (Fig. 8H).
313 In bacteria originating from WT microcolonies incubated with unprimed BMDMs, there were
314 low levels of fluorescence from the *Phmp::mcherry* reporter (Fig. 8H: left, no treatment). After
315 challenge with LPS/IFNγ-primed BMDMs, there was increased *hmp* expression, with a small
316 percentage of the population expressing high levels of the *Phmp::mcherry* reporter (Fig. 8H left,
317 LPS/ IFNγ). Inhibition of activated BMDMs with NMMA resulted in a peak that was almost
318 indistinguishable from the bacteria exposed to unprimed BMDMs (Fig. 8H left, L-NMMA +
319 LPS/ IFNγ). Bacteria that originated from *Δhmp* microcolonies showed uniformly high

fluorescence contours for *Phmp::mcherry* after challenge with LPS/IFNγ-primed BMDMs, showing that NO secreted by macrophages can penetrate the entire microcolony (Fig. 8H: right). As expected, there was low *Phmp::mcherry* fluorescence after challenge with unprimed BMDMs and NOS-inhibited BMDMs (Fig. 8H right; L-NMMA + LPS/ IFNγ). In summary, peripheral expression of *hmp* in WT droplet microcolonies was dependent upon challenge with LPS/IFNγ-primed BMDMs and mimicked the bacterial response to recruited innate immune cells observed in mouse tissue.

Discussion

Many invasive bacterial pathogens can colonize hosts and disseminate to both peripheral and deep tissue sites where they establish replicative niches. For pathogens as diverse as *Mycobacterium tuberculosis* and *Staphylococcus aureus*, growth in tissues is followed by recruitment of neutrophils, macrophages and inflammatory monocytes, which can lead to the formation of abscesses or granulomas when the infection is not eradicated (Cheng et al., 2011; Pagan & Ramakrishnan, 2018). These pathogen-immune cell aggregates are intricate structures in which the pathogen interfaces with host cells, but also result in significant self and social interactions, making it difficult to reproduce in culture the entire set of events present in tissue. Although there is considerable research on infectious lesions caused by these pathogens, there are few informative culture models that reconstruct the pathogen-immune cell architecture occurring in tissues that preserve inter-microbial interactions (Elkington et al., 2019; Fitzgerald et al., 2014; Fonseca et al., 2017; Guggenberger et al., 2012; Guirado et al., 2015).

We have addressed this gap in the field by reconstructing *Yptb* inflammatory sites using microfluidic technology to generate a 3D model that allows interbacterial interactions to be

studied as well as action-at-a-distance by immune cells, with topology mimicking a tissue infection. *Yptb* is an intestinal pathogen that can establish extracellular foci in deep tissue sites after translocation across the intestine into either the bloodstream or regional lymph nodes (Barnes et al., 2006). In the course of establishing an infectious niche within the murine spleen, *Yptb* forms microcolonies tightly associated with recruitment of neutrophils that directly contact the cluster of bacteria, which are, in turn, encased by layers of more neutrophils followed by macrophages and monocytes that largely do not contact bacteria directly (Davis et al., 2015). The model system developed here closely mimics this topology. Droplets support the growth of *Yptb* microcolonies, and activated BMDMs localized at a similar distance to that observed in tissues drive a bacterial transcriptional response that recapitulates interactions observed in tissue. Associated with the recruitment of immune cells to infection is the presence of $iNOS^+$ cells that are clearly activated to express iNOS and release NO. These cells do not directly contact the growing colony, so their ability to modulate microbial growth would appear to be linked to the production of soluble anti-microbial mediators. In concert with attack-from-a-distance, there is an outer shell of bacteria protecting the microcolony from RNI attack by producing the detoxifying Hmp protein that clearly responds to this stress without directly contacting $iNOS^+$ cells. To mimic clonal growth in the spleen and action at distance, our tissue culture system used microfluidics-generated droplets, which allowed us to maximize the capture of single bacteria within 65µm agarose/ HyStem®-C Hydrogel droplets and allow adhesion of macrophages on the droplet surface. The bacteria appeared to tolerate being encompassed in this environment as evident by *Yptb* replication, allowing a reasonable facsimile of spleen-resident microcolonies. In addition to the cells analyzed here, neutrophils are present surrounding the cluster of *Yptb*, but only a few peripheral bacteria are in direct contact with these cells, with the consequence that

366 they are largely inhibited by translocated TTSS effector proteins. Future work will involve
367 modifying the system to allow the incorporation of neutrophils, so that the response of bacteria
368 on the extreme periphery of the colony can be analyzed during this process. This will involve
369 either embedding cells in the droplet matrix, or forcing controlled degradation of the matrix to
370 allow close contact with the microcolony (Guggenberger et al., 2012; Sakai et al., 2012).
371 One of the surprising results from this study was that we could totally reproduce
372 topologically driven regulation of the *hmp* promoter by incubating droplet-encased
373 microcolonies in the presence of the NO generator DETA-NONOate. This indicates that
374 production of RNI by iNOS$^+$ cells does not require directional targeting of the bacteria by these
375 cells, but rather is a consequence of multi-cell collaboration to generate toxic amounts of RNI,
376 with the concentrations determined by the total number of recruited iNOS$^+$ cells. By
377 encompassing the infection site, the sum of the RNI produced by individual cells generates a
378 sufficient amount of chemical to induce transcription of the reporter construct and kill bacterial
379 mutants unable to produce Hmp.
380 To demonstrate that the addition of this chemical could reconstruct RNI signaling within
381 the bacterial colony, we developed a script that could be used to quantify the accumulation of a
382 fluorescence signal around the periphery of microcolonies. This strategy demonstrated that the
383 use of DETA-NONOate was sufficient to generate a robust response on the periphery relative to
384 a region internal to the colony that defined the area of lowest fluorescence intensity. It also
385 demonstrated that the gradient of *Phmp* expression depends on both iNOS$^+$ activity and overall
386 activation of macrophages by LPS and IFNγ. Based on quantification of this ratio, we would
387 argue that addition of BMDMs to the droplets generated somewhat lower amount of RNI than
388 resulted from 1 mM DETA-NONOate (compare Figs. 6A to 8G). It would be difficult to directly

compare these results to mouse tissue, as the nature of the samples and preservation technique differs greatly from the droplet analysis. It does argue that the amount of RNI generated by 1 mM DETA-NONOate is more than sufficient to explain the images generated from the mouse spleen.

One of the strengths of the synthetic droplet system is that we were able to disrupt the droplets to free the bacteria and analyze bacterial populations in bulk, a task that is often difficult to perform when isolating colonies from mammalian tissues. Once the colonies were disrupted, we demonstrated that individual cells can be subjected to flow cytometry analysis, allowing the response of spatially distinct population of bacteria to be analyzed. This approach should facilitate identifying additional macrophage secreted products that can penetrate microcolonies and control bacterial gene expression. There are a variety of small secretory molecule products of macrophages that have been identified, but the roles of these products in controlling bacterial growth or modulating gene expression of microorganisms is greatly understudied (Nathan, 1987; Sugimoto et al., 2011). Presumably, transcriptional analysis of bacterial subpopulations will facilitate dissection of previously unappreciated bacterial responses to the host and potentially identify new host strategies for restricting microbial growth.

Materials and Methods

Bacterial strains & growth conditions. All experiments used derivatives of the *Y. pseudotuberculosis* strain IP2666 (Balada-Llasat & Mecsas, 2006). For all droplet experiments, bacteria were grown overnight into stationary phase in 2xYT broth (Crimmins et al., 2012; Davis et al., 2015) at 26 ºC with rotation. Overnight cultures were diluted 1:2000 in 1% ultra-low-melt agarose (Sigma, USA, #A2576) in 2xYT containing 25% Hystem®-C hydrogel kit (ESI BIO,

412 CA, USA, #GS312) prior to droplet generation. For broth nitric oxide exposure, overnight
413 cultures were diluted 1:100 in 2xYT and rotated at 26 ºC for the indicated times.

414 ***Generation of plasmid-based reporter strains***. The *Y. pseudotuberculosis* reporter strains
415 in this study have been previously described (Crimmins et al., 2012; Davis et al., 2015). GFP^+
416 strains express GFP from the unrepressed *PTet* promoter of pACYC184 (Chang & Cohen, 1978).
417 The *Phmp::mCherry* transcriptional fusion was constructed by fusing the *hmp* promoter to
418 *mCherry* using overlap extension PCR, and cloning into the pMMB67EH plasmid (Jens P.
419 Fiirstea, 1986). Strains that express both reporters are co-transformants of the compatible
420 pACYC184 and pMMB67EH plasmids.

421 ***Droplet generation***. CAD-designed microfluidics chips having 38 independent devices
422 controlled by two input ports were constructed according to published protocols (Mazutis et al.,
423 2013; Thibault et al., 2019) at the Boston College Nanofabrication Facility
424 (https://www.bc.edu/bc-web/schools/mcas/sites/cleanroom.html). After construction, each
425 microfluidics chip was stored at 37 ºC in a box with the chip covered in tape. Prior to droplet
426 generation, the device was primed with fluorinated oil (3M, USA, Novec 7500) and connected to
427 two programmable syringe pumps (Harvard Apparatus 11 Elite Series) located in a temperature-
428 controlled room at 37 ºC. One pump was fitted with a 1ml syringe (BD, NJ, USA, #309628)
429 having a 27-gauge needle (BD #305109), which was filled with 1.5% Pico-Surf 1 (Dolomite
430 Microfluidics, MA, USA, 5% in Novec 7500) in Novec 7500 oil. In parallel, bacteria were
431 diluted 1:2000 in 1% ultra-low-melt agarose containing Hystem-C® hydrogel, yielding
432 approximately 5 x 10^6 cells/ml, and the mix was loaded into a 1 ml syringe that was fitted onto a
433 second pump. Polyethylene (PE/2) tubing (SCI COM, AZ, USA, #BB31695-PE/2) was attached
434 to each syringe and then inserted into the appropriate ports on the microfluidics device (Fig. 1).

435 The pump holding the oil-phase was set to 700 µl/hour while the other pump was set to 400
436 µl/hour and droplets were collected in a 1.5 ml Eppendorf tube through tubing that had been
437 inserted into the droplet collection port.

438 ***Oil Removal.*** 100 µl of droplets was introduced into a 1.5 ml Eppendorf tube and 500 µl
439 of 10% 1H,1H,2H,2H-Perfluoro-1-octanol (PFO) (Sigma #370533-25G) in Novec 7500 was
440 added to the droplets. After mixing vigorously, the tube was placed in a centrifuge for 30
441 seconds at 250 RCF and 400 µl of 25% Extralink (ESI BIO #GS3006) in PBS was added to
442 crosslink the hydrogel within the agarose. After crosslinking, the droplets were flicked into
443 suspension and centrifuged for 30 seconds at 250 RCF. The PBS/droplet layer was transferred to
444 a new 1.5 ml Eppendorf tube, subjected to centrifugation for 30 seconds at 250 RCF, and washed
445 with PBS. The remaining droplets were resuspended in 2xYT broth.

446 ***Droplet dispersal.*** Droplets were washed once in PBS at the indicated timepoints,
447 incubated for 3 minutes at 50 °C, and a mixture of agarase (Sigma #A6306), collagenase and
448 hyaluronidase (StemCell Technology, MA, USA, #07912) was added to the samples for 45
449 minutes at 37 °C. Samples were then incubated for 3 minutes at 60 °C, subjected to centrifugation
450 in a microfuge at 14K RPM for 1 minute. The supernatant was then aspirated, and the bacterial
451 pellets were washed in PBS and prepared for flow analysis.

452 ***Nitric oxide experiments.*** To analyze the response of colonies to exogenous NO, droplets
453 containing *Y. pseudotuberculosis* were generated, oil was removed, and the droplets were rotated
454 for 7 hours at 26 °C in 2xYT broth to allow colony formation. After the 7-hour growth period,
455 droplets were subjected to centrifugation for 30 seconds at 250 RCF and washed twice in PBS.
456 50 µl of droplets were transferred to a 1.5 ml Eppendorf tube and resuspended in 1 ml 2xYT

457 broth and exposed to DETA-NONOate (Sigma #AC32865) during growth at 26 ºC with aeration
458 for the indicated timepoints. For experiments performed at 37 °C with 5% CO_2 (Fig. 5), 50 µl of
459 droplets were resuspended in 1 ml RPMI 1640 (Gibco, USA) supplemented with 10% FBS and 2
460 mM glutamine media in 12- well non-tissue culture treated plates for the indicated times.

461 ***Isolation of bone marrow-derived macrophages.*** Bone marrow cells were isolated from
462 femurs, tibias, and humeri of female 6-8-week-old C57BL/6 mice, and terminally differentiated
463 into macrophages in medium containing mouse CSF generated as previously described
464 (Auerbuch et al., 2009). Bone marrow-derived macrophages (BMDMs) were subsequently
465 frozen in fetal bovine serum (FBS) with 10% dimethyl sulfoxide (DMSO) and plated one day
466 prior to incubation with droplets in 90% fresh medium (RPMI 1640 (Gibco) supplemented with
467 10% FBS and 2 mM glutamine) spiked with 10% sterile medium containing macrophage colony
468 stimulating factor (MCSF) in 5% CO_2 at 37ºC. Medium containing MCSF was conditioned by
469 growth in the presence of mouse 3T3 fibroblasts that overproduce mouse MCSF at 37 °C with
470 5% CO2, as previously described (Auerbuch et al., 2009; Leber et al., 2008). To stimulate
471 BMDMs to induce iNOS expression, cells from frozen stocks were plated on non-tissue culture
472 treated plates and allowed to recover overnight. The following day, BMDMs were stimulated
473 with 200 U/ml IFNγ (Peprotech, NJ, USA) and 100 ng/ml LPS (Sigma) for 12-15 hours (Mosser
474 & Gonçalves, 2015). For inhibition of iNOS, BMDMs were incubated with 2 mM NG-
475 Monomethyl-L-arginine monoacetate (L-NMMA) (Acros Organics, NJ, USA) one day prior to
476 priming with LPS and IFNγ (Frawley et al., 2018).

477 ***Droplet-BMDM experiments.*** Droplets containing *Y. pseudotuberculosis* were generated,
478 oil was removed, and the droplet-encased bacteria were grown with aeration for 7 hours at 26 ºC
479 in 2xYT broth. After the 7-hour growth period, droplets were pelleted for 30 seconds at 250

RCF, washed twice in PBS and supernatant was removed. 50 µl of droplets were transferred to a well in a 12-well coverslip-bottom plate (Cellvis, CA, USA, #P12-1.5H-N), approximately 2 x 10^6 BMDMs in RPMI 1640 supplemented with 10% FBS and 2 mM glutamine were added to the well, and the incubation proceeded at 37 °C in the presence of 5% CO_2 for 4 hours. Samples were fixed in 2% paraformaldehyde (PFA) in PBS, washed in PBS, and fluorescent reporters were visualized by microscopic observation.

Murine model of systemic infection. Six to 8-week old female C57BL/6 mice obtained from Jackson Laboratories (Bar Harbor, ME) were injected intravenously with 10^3 bacteria. Three days post inoculation, spleens were removed and processed as described previously (Crimmins et al., 2012; Davis et al., 2015). All animal studies were approved by the Institutional Animal Care and Use Committee of Tufts University.

Flow cytometry. After microcolony dispersal, samples were fixed in 2% PFA in PBS, washed in PBS, and filtered through 40 µm filters. Fluorescent reporters were detected using a Bio-Rad S3e cell sorter. 100,000 events were collected for each sample.

Fluorescence microscopy. After 4 hours of nitric oxide exposure or challenge with BMDMs, droplets were fixed in 2% PFA in PBS for 10 minutes. Droplets that were exposed to the nitric oxide donor were mounted in 8 well chamber slides using ProLong Gold (Life Technologies, CA, USA). Droplets that were incubated with BMDMs were visualized in 12-well coverslip-bottom plates (Cellvis). For visualization of BMDMs, cells were fixed in 2% PFA in PBS, permeabilized for 30 seconds in ice cold methanol and non-specific binding was blocked using 2% BSA in PBS. Cells were stained with rabbit anti-mouse iNOS (Abcam, MA, USA) at a dilution of 1:100 and goat anti-rabbit-Alexa 488 (Invitrogen, CA, USA) at a dilution of 1:500.

Nuclei were stained with Hoechst at a dilution of 1:10,000. To analyze tissue samples, C57BL/6 mice were inoculated intravenously with the WT *gfp+ Phmp::mcherry* strain. Three days post inoculation, spleens were harvested and fixed in 4% PFA in PBS for 3 hours, tissue was frozen embedded in Sub Xero freezing media (Mercedes Medical, FL, USA) and cut into 10 µm sections using a cryostat microtome (Microm HM505E). To visualize reporters, sections were thawed in PBS, stained with Hoechst at a 1:10,000 dilution, washed in PBS, and coverslips were mounted using ProLong Gold (Life Technologies). Tissue was imaged with a 63x objective on a Zeiss Axio Observer.Z1 (Zeiss) microscope with Colibri.2 LED light source, an Apotome.2 (Zeiss) for optical sectioning, and an ORCA-R^2 digital CCD camera (Hamamatsu) (Crimmins et al., 2012; Davis et al., 2015).

Determination of droplet size, bacterial counts and microcolony area. For determination of droplet size, images were captured by phase contrast microscopy using a 20x lens, and images were analyzed to identify 300 droplets, with analysis in Volocity™. Droplet size was determined by identifying a threshold that defines edges of droplets and determining the diameter in pixels. The data were then converted to metric scale using a stage micrometer and displayed as a histogram. To determine bacterial counts, images were captured by phase contrast and fluorescence microscopy using a 20x lens and the number of bacteria/droplet was manually counted in 500 droplets. To determine microcolony area, images were captured by phase contrast and fluorescence microscopy using a 20x lens with analysis in Volocity™. Microcolony area was determined by identifying a threshold that defines edges of microcolonies in the GFP channel and determining the number of pixels in the region of interest (ROI). The data were then converted to metric scale using a stage micrometer and displayed as μm^2.

524 ***Quantitative mage analysis***. MATLAB scripts were written to calculate the average
525 intensity of fluorescence about the periphery of microcolonies and point of lowest fluorescence
526 (https://github.com/isberg-lab/droplet). Periphery to point of lowest intensity (PLI) ratios were
527 calculated by generating a mask representing the periphery of a defined width of the
528 microcolony, and a mask representing the PLI of a defined radius. The periphery mask was
529 generated by first thresholding the green channel using Otsu's method and converting the
530 resulting matrix into a binary matrix. The binary matrix was morphologically opened with a
531 disk-shaped structuring element of radius two and then morphologically closed with a disk-
532 shaped structuring element of radius four. Morphologic opening and closing eliminate dim
533 artifacts and fuse the microcolony mask into a single region of interest (ROI). Any remaining
534 holes within contiguous ROIs are filled. ROIs touching the edge of the field are removed, as are
535 all but the largest ROI in the field. This ROI, covering the entire microcolony, is eroded with a
536 disk-shaped structuring element of radius 12 and complemented. The initial mask and
537 complemented eroded mask are combined to achieve a binary mask of the periphery of the
538 object. The number of pixels and the total intensity in the resulting mask was recorded. The mask
539 was applied to the raw image data in the red channel, and the total intensity was recorded. Total
540 intensity of the red was normalized to the number of pixels to achieve an average intensity for
541 the entire periphery. The average intensity of the red channel was normalized to the average
542 intensity of the green channel. To calculate the PLI, the determined eroded mask was applied to
543 the red channel to isolate the pixels belonging to the microcolony while excluding those that are
544 part of the periphery. A Gaussian blur of sd = 2.0 was applied to reduce the effects of low-
545 intensity noise introduced by the imaging process. The coordinates of the minimum value of this
546 image were calculated, generating a binary matrix with value = 1 at the coordinates of the PLI

and zero at all other points. This matrix was morphologically dilated with a structuring element of radius 5 to sample a region of lowest intensity rather than a single pixel. The number of pixels in this resulting mask are then recorded and the total intensity of the green channel was recorded. The mask was applied to the raw image data in the red channel, and the total intensity recorded. Total intensity was normalized to number of pixels to achieve an average intensity for the entire PLI region in the red and this value was normalized to the average intensity of the green channel.

Acknowledgements. The work in this study was supported by NIAID grants R01 AI110684 and R21 151593 to RRI and U01AI124302 and R01 AI110724 to TvO. SC and LS were supported by predoctoral training grant T32 TM007310 from NIGMS. We thank the Boston College Integrated Sciences Nanofabrication Facility for support and thank Kristen Davis, Efrat Hamami and Wenwen Huo for review of the manuscript.

Figure Legends

Figure 1. Droplet gels support clonal growth of *Yersinia pseudotuberculosis.* A. *Y. pseudotuberculosis* was added to molten agarose/HyStem®-C Hydrogel and introduced into a microfluidics device, allowing encapsulation within oil-coated droplets (Materials and Methods). Oil was removed from the droplets and bacteria were cultured *in situ* within the droplets (Thibault et al., 2019). B. Design of the microfluidics device. Noted are oil and aqueous (molten gel/bacteria mixture) phase inlets (red and blue arrows, respectively). Droplets were collected into a tube at the droplet output (black arrow) (Thibault et al., 2019). C. Distribution of droplet sizes prior to oil removal. Droplet size was determined by capturing images from phase contrast microscopy followed by image processing (Materials and Methods). D, E. Droplets largely contain one or two bacterial cells immediately after encapsulation. D. Image of droplets containing *Y. pseudotuberculosis gfp*$^{+}$. E. Presence of bacteria was scored immediately after encapsulation by phase contrast and fluorescence microscopy, scoring for GFP. F. *Y. pseudotuberculosis* grows within colonies in droplets. Droplets containing encapsulated *Y. pseudotuberculosis* were cultured at 26ºC, and microcolonies were visualized at indicated timepoints by phase contrast and fluorescence microscopy. Microcolony areas were determined by image analysis (Materials and Methods). Each timepoint is median +/- 95% confidence interval (CI) of 3 biological replicates of 50 microcolonies. G. Representative images of microcolonies from (F) at the noted times visualized by phase contrast and fluorescence microscopy. Scale bar: 50μm.

Figure 2. Droplet-generated *Yersinia pseudotuberculosis* microcolonies require Hmp to maintain growth in presence of NO. Indicated *Y. pseudotuberculosis* strains were cultured in

583 2xYT with rotation at 26 ºC for 7 hours prior to DETA-NONOate exposure. At the indicated
584 timepoints, an aliquot of droplets was fixed and visualized by fluorescence microscopy. (A, D).
585 Microcolony area determined from captured images followed by image analysis (Materials and
586 Methods). Each point represents a single droplet with median noted. (B, E). Representative WT
587 (B) and Δ*hmp* (E) microcolonies after 8 hours of treatment with and without DETA-NONOate.
588 Scale bar: 50μm. (C, F). Overnight broth cultures of *Y. pseudotuberculosis* were diluted 1:10 in
589 2xYT broth prior to addition of DETA-NONOate. At indicated timepoints, culture density was
590 determined (Materials and Methods).

591

592 **Figure 3. Topological constraints drive non-uniform expression of *hmp*.** (A). Model of the
593 predicted outcome for the nitric oxide (NO) response of *Y. pseudotuberculosis* grown in broth
594 versus droplet culture (Davis et al., 2015). Red: bacteria showing high expression of P_{hmp}-
595 *mCherry* reporter. White: bacteria showing undetectable mCherry fluorescence. (B, C). *Y.*
596 *pseudotuberculosis* grown in droplet microcolonies show altered response to NO. Noted
597 bacterial strains harboring gfp^{+} P_{hmp}-*mcherry* plasmids were grown in either broth (open
598 histograms) or droplets (filled histograms) in the presence of NO donor for the noted times.
599 Droplet microcolonies were dispersed at noted times and analyzed by flow cytometry (Materials
600 and Methods). B. Flow analysis of mCherry channel. C. Analysis of GFP channel.

601

602 **Figure 4. Spatial regulation of *hmp* expression in tissues can be reproduced in droplet**
603 **culture.** (A). Experimental overview. Droplets seeded with *Y. pseudotuberculosis* harboring
604 fluorescence reporters were incubated for 7 hours at 26 ºC and varying concentrations of DETA-

NONOate were added to the cultures for 4 hours at 37 ºC, 5% CO_2. After 4 hours, the droplets were fixed and visualized using brightfield and fluorescence microscopy. (B, C). Representative WT and Δ*hmp* microcolonies after 4 hours of treatment with 1mM DETA-NONOate.

Figure 5. Strategy for quantification of *hmp* expression localized on periphery of microcolonies. A. Design of script that allows the identification of regions of interest (ROIs) for the purpose of determining the average fluorescence intensities and normalization strategies within the ROIs. Script defines periphery of microcolony and sets mask, allowing a user-defined width extending into the microcolony along with a point of lowest intensity (PLI) which is determined based on the mCherry signal for each microcolony. The fluorescence at the periphery is calculated as a ratio of the average pixel intensity of the mcherry channel in periphery divided by the average pixel intensity of the GFP channel in the periphery, allowing normalization for bacterial expression. The fluorescence for the defined PLI is also calculated in the same fashion, and the periphery verses PLI ratio is determined (Supplemental Data). B. Example of identification of periphery, mask generation and definition of peripheral ROI. The GFP channel defines the periphery, allowing mask to be set. Within the mask, the periphery is defined as extending 12 pixels into the microcolony. The PLI within the mask is defined as the area of 5-pixel radius with the lowest intensity in the mCherry channel.

Figure 6. Hmp activity is required for peripheral expression of *hmp* in response to NO. (A-C). The presence of Hmp activity is required for *Y. pseudotuberculosis* to have enhanced expression of P_{hmp} in microcolonies exposed to NO. A. Periphery versus PLI ratio for

627 microcolonies as a function of DETA-NONOate concentration in microcolonies from noted
628 bacterial strains. B. Microcolony area (pixels^2) for WT and Δ*hmp* microcolonies at different
629 concentrations of DETA-NONOate. Black circles: 100 individual microcolonies measured for
630 each condition. Lines indicate the medians. (C). Flow cytometric analysis of dispersed
631 microcolonies. Droplets were dispersed into single cells after 4 hours of DETA-NONOate
632 treatment at noted concentrations and subjected to flow cytometry (Materials and Methods).
633 Bacteria were gated for GFP$^+$ and analyzed for mCherry signal. Statistics: Mann-Whitney test,
634 ****p<0.0001, ns: not significant.

635

636 **Figure 7. Recruitment of iNOS$^+$ cells is associated with the maturation of *Yersinia***
637 ***pseudotuberculosis* microcolonies in tissue.** A. C57BL/6 mice were inoculated intravenously
638 (i.v.) with 10^3 WT *gfp*+ bacteria, and spleens were harvested 3 days post-inoculation (PI). Spleen
639 tissue was probed with α-Ly6G and α-iNOS and visualized by fluorescence microscopy.
640 Neutrophils (α-Ly6G$^+$; red) surround a cluster of *Y. pseudotuberculosis* (green). Surrounding the
641 sphere of bacteria that is encased by neutrophils (white circle) is a layer of iNOS+ cells. White
642 arrows: The distance between *Y. pseudotuberculosis* and the iNOS+ cell layer (not to scale). B.
643 Model for droplet microcolonies. Bacteria are grown *in situ* within the droplets prior to challenge
644 with iNOS$^+$ cells to mimic *Y. pseudotuberculosis* microcolony structure in tissue. Black arrows
645 note there is space between iNOS+ cells and cluster of bacteria.

646

647 **Figure 8. Activated BMDMs drive peripheral expression of *hmp* in droplet microcolonies,**
648 **mimicking tissue spatial regulation.** A. Experimental overview. Droplets containing *Y.*

649 *pseudotuberculosis* were grown for 7 hours at 26 ºC prior to incubation with BMDMs for 4 hours
650 at 37 ºC, CO_2. The fixed microcolonies were visualized using brightfield and fluorescence
651 microscopy and subjected to image analysis (Materials and Methods). B. Resting BMDMs (left)
652 and LPS/IFNγ-primed BMDMs (right) were fixed, probed with α-iNOS and visualized by
653 fluorescence microscopy. (C). C57BL/6 mice were inoculated intravenously (i.v.) with 10^3 WT
654 *gfp+* P_{hmp}-*mcherry* bacteria, and spleens were harvested 3 days post-inoculation (PI) for
655 fluorescence microscopy. A representative microcolony from tissue is shown. (D, E).
656 Representative WT (D) and Δ*hmp* (E) microcolonies incubated with LPS/IFNγ-primed BMDMs.
657 (F). Microcolony area in presence of BMDMs, incubated as noted. (G) Periphery verses PLI
658 ratios for microcolonies incubated with BMDMs treated as noted. Black circles: 100 individual
659 microcolonies from each condition. Line indicates median. (H). Flow cytometry of dispersed
660 microcolonies after 4 hours of incubation with BMDMs. Dispersed bacteria were gated for GFP^+
661 and mCherry fluorescence was determined (Materials and Methods). Statistics: Mann-Whitney
662 test, ****p<0.0001, ***p<0.0005, **p<0.005, *p<0.05, ns: not significant.

663

664 **Figure S1. Topological constraints drive non-uniform expression of *hmp*.** (A-D). *Y.*
665 *pseudotuberculosis* grown in droplet microcolonies show altered response to NO. Noted
666 bacterial strains harboring gfp^+ P_{hmp}-*mcherry* plasmids were grown in either broth (open
667 histograms) or droplets (filled histograms) in the presence of NO donor for the noted times.
668 Droplet microcolonies were dispersed at noted times and analyzed by flow cytometry (Materials
669 and Methods). A. Flow analysis of mCherry channel from WT. B. Analysis of GFP channel from
670 WT. C. Flow analysis of mCherry channel from Δhmp. C. Analysis of GFP channel from *Δhmp*.

671

672

673 **References**

674 Auerbuch, V., Golenbock, D. T., & Isberg, R. R. (2009). Innate immune recognition of Yersinia
675 pseudotuberculosis type III secretion. *PLoS Pathog, 5*(12), e1000686.
676 doi:10.1371/journal.ppat.1000686
677 Balada-Llasat, J. M., & Mecsas, J. (2006). Yersinia has a tropism for B and T cell zones of
678 lymph nodes that is independent of the type III secretion system. *PLoS Pathog, 2*(9), e86.
679 doi:10.1371/journal.ppat.0020086
680 Barnes, P. D., Bergman, M. A., Mecsas, J., & Isberg, R. R. (2006). Yersinia pseudotuberculosis
681 disseminates directly from a replicating bacterial pool in the intestine. *J Exp Med, 203*(6),
682 1591-1601. doi:10.1084/jem.20060905
683 Bogdan, C. (2001). Nitric oxide and the immune response. *Nat Immunol, 2*(10), 907-916.
684 doi:10.1038/ni1001-907
685 Carter, P. B., & Collins, F. M. (1974). The route of enteric infection in normal mice. *J Exp Med,*
686 *139*(5), 1189-1203. doi:10.1084/jem.139.5.1189
687 Cha, B. H., Shin, S. R., Leijten, J., Li, Y. C., Singh, S., Liu, J. C., . . . Khademhosseini, A.
688 (2017). Integrin-Mediated Interactions Control Macrophage Polarization in 3D
689 Hydrogels. *Adv Healthc Mater, 6*(21). doi:10.1002/adhm.201700289
690 Chang, A. C., & Cohen, S. N. (1978). Construction and characterization of amplifiable
691 multicopy DNA cloning vehicles derived from the P15A cryptic miniplasmid. *Journal of*
692 *Bacteriology, 134*(3), 1141-1156. Retrieved from
693 https://jb.asm.org/content/jb/134/3/1141.full.pdf
694 Cheng, A. G., DeDent, A. C., Schneewind, O., & Missiakas, D. (2011). A play in four acts:
695 Staphylococcus aureus abscess formation. *Trends Microbiol, 19*(5), 225-232.
696 doi:10.1016/j.tim.2011.01.007
697 Cheng, A. G., Kim, H. K., Burts, M. L., Krausz, T., Schneewind, O., & Missiakas, D. M. (2009).
698 Genetic requirements for Staphylococcus aureus abscess formation and persistence in
699 host tissues. *FASEB J, 23*(10), 3393-3404. doi:10.1096/fj.09-135467
700 Crimmins, G. T., Mohammadi, S., Green, E. R., Bergman, M. A., Isberg, R. R., & Mecsas, J.
701 (2012). Identification of MrtAB, an ABC transporter specifically required for Yersinia
702 pseudotuberculosis to colonize the mesenteric lymph nodes. *PLoS Pathog, 8*(8),
703 e1002828. doi:10.1371/journal.ppat.1002828
704 Davis, K. M., Mohammadi, S., & Isberg, R. R. (2015). Community behavior and spatial
705 regulation within a bacterial microcolony in deep tissue sites serves to protect against
706 host attack. *Cell Host Microbe, 17*(1), 21-31. doi:10.1016/j.chom.2014.11.008
707 Elkington, P., Lerm, M., Kapoor, N., Mahon, R., Pienaar, E., Huh, D., . . . Schlesinger, L. S.
708 (2019). In Vitro Granuloma Models of Tuberculosis: Potential and Challenges. *J Infect*
709 *Dis, 219*(12), 1858-1866. doi:10.1093/infdis/jiz020
710 Fitzgerald, L. E., Abendano, N., Juste, R. A., & Alonso-Hearn, M. (2014). Three-dimensional in
711 vitro models of granuloma to study bacteria-host interactions, drug-susceptibility, and
712 resuscitation of dormant mycobacteria. *Biomed Res Int, 2014*, 623856.
713 doi:10.1155/2014/623856

Fonseca, K. L., Rodrigues, P. N. S., Olsson, I. A. S., & Saraiva, M. (2017). Experimental study of tuberculosis: From animal models to complex cell systems and organoids. *PLoS Pathog, 13*(8), e1006421. doi:10.1371/journal.ppat.1006421

Frawley, E. R., Karlinsey, J. E., Singhal, A., Libby, S. J., Doulias, P.-T., Ischiropoulos, H., & Fang, F. C. (2018). Nitric Oxide Disrupts Zinc Homeostasis in Salmonella enterica Serovar Typhimurium. *mBio, 9*(4), e01040-01018. doi:10.1128/mBio.01040-18

Freund, S., Czech, B., Trulzsch, K., Ackermann, N., & Heesemann, J. (2008). Unusual, virulence plasmid-dependent growth behavior of Yersinia enterocolitica in three-dimensional collagen gels. *J Bacteriol, 190*(12), 4111-4120. doi:10.1128/JB.00156-08

Giancotti, F. G., & Ruoslahti, E. (1999). Integrin Signaling. *Science, 285*, 1028-1033.

Green, S. J., Aniagolu, J., & Raney, J. J. (1994). Oxidative Metabolism of Murine Macrophages. *Current Protocols in Immunology, 12*(1), 14.15.11-14.15.11. doi:10.1002/0471142735.im1405s12

Guggenberger, C., Wolz, C., Morrissey, J. A., & Heesemann, J. (2012). Two distinct coagulase-dependent barriers protect Staphylococcus aureus from neutrophils in a three dimensional in vitro infection model. *PLoS Pathog, 8*(1), e1002434. doi:10.1371/journal.ppat.1002434

Guirado, E., Mbawuike, U., Keiser, T. L., Arcos, J., Azad, A. K., Wang, S. H., & Schlesinger, L. S. (2015). Characterization of host and microbial determinants in individuals with latent tuberculosis infection using a human granuloma model. *mBio, 6*(1), e02537-02514. doi:10.1128/mBio.02537-14

Jens P. Fiirstea, W. P., Ronald Frank, Helmut Blbcker, Peter Scholz, Michael Bagdasarian, and Erich Lanka. (1986). Molecular cloning of the plasmid RP4 primase region in a multi-host-range tacP expression vector. *Gene, 48*, 119-131.

Koster, S., Angile, F. E., Duan, H., Agresti, J. J., Wintner, A., Schmitz, C., . . . Weitz, D. A. (2008). Drop-based microfluidic devices for encapsulation of single cells. *Lab Chip, 8*(7), 1110-1115. doi:10.1039/b802941e

Leber, J. H., Crimmins, G. T., Raghavan, S., Meyer-Morse, N. P., Cox, J. S., & Portnoy, D. A. (2008). Distinct TLR- and NLR-mediated transcriptional responses to an intracellular pathogen. *PLoS Pathog, 4*(1), e6. doi:10.1371/journal.ppat.0040006

MacMicking, J. D., North, R. J., LaCourse, R., Mudgett, J. S., Shah, S. K., & Nathan, C. F. (1997). Identification of nitric oxide synthase as a protective locus against tuberculosis. *Proc Natl Acad Sci U S A, 94*(10), 5243-5248. doi:10.1073/pnas.94.10.5243

Macosko, E. Z., Basu, A., Satija, R., Nemesh, J., Shekhar, K., Goldman, M., . . . McCarroll, S. A. (2015). Highly Parallel Genome-wide Expression Profiling of Individual Cells Using Nanoliter Droplets. *Cell, 161*(5), 1202-1214. doi:10.1016/j.cell.2015.05.002

Mazutis, L., Gilbert, J., Ung, W. L., Weitz, D. A., Griffiths, A. D., & Heyman, J. A. (2013). Single-cell analysis and sorting using droplet-based microfluidics. *Nat Protoc, 8*(5), 870-891. doi:10.1038/nprot.2013.046

Mosser, D. M., & Gonçalves, R. (2015). Activation of Murine Macrophages. In *Current Protocols in Immunology* (pp. 14.12.11-14.12.10).

Murray, H. W., & Nathan, C. F. (1999). Macrophage microbicidal mechanisms in vivo: reactive nitrogen versus oxygen intermediates in the killing of intracellular visceral Leishmania donovani. *J Exp Med, 189*(4), 741-746. doi:10.1084/jem.189.4.741

759 Nathan, C. F. (1987). Secretory products of macrophages. *J Clin Invest, 79*(2), 319-326.
760 doi:10.1172/JCI112815
761 Pagan, A. J., & Ramakrishnan, L. (2018). The Formation and Function of Granulomas. *Annu Rev*
762 *Immunol, 36*, 639-665. doi:10.1146/annurev-immunol-032712-100022
763 Poole, R. K., Anjum, M. F., Membrillo-Hernández, J., Kim, S. O., Hughes, M. N., & Stewart, V.
764 (1996). Nitric oxide, nitrite, and Fnr regulation of hmp (flavohemoglobin) gene
765 expression in Escherichia coli K-12. *Journal of Bacteriology, 178*(18), 5487-5492.
766 doi:10.1128/jb.178.18.5487-5492.1996
767 Poole, R. K., & Hughes, M. N. (2000). New functions for the ancient globin family: bacterial
768 responses to nitric oxide and nitrosative stress. *Mol Microbiol, 36*(4), 775-783.
769 doi:10.1046/j.1365-2958.2000.01889.x
770 Robinson, J. L., & Brynildsen, M. P. (2013). A kinetic platform to determine the fate of nitric
771 oxide in Escherichia coli. *PLoS Comput Biol, 9*(5), e1003049.
772 doi:10.1371/journal.pcbi.1003049
773 Sakai, S., Inagaki, H., Inamoto, K., & Taya, M. (2012). Wrapping tissues with a pre-established
774 cage-like layer composed of living cells. *Biomaterials, 33*(28), 6721-6727.
775 doi:10.1016/j.biomaterials.2012.06.027
776 Shiloh, M. U., MacMicking, J. D., Nicholson, S., Brause, J. E., Potter, S., Marino, M., . . .
777 Nathan, C. (1999). Phenotype of mice and macrophages deficient in both phagocyte
778 oxidase and inducible nitric oxide synthase. *Immunity, 10*(1), 29-38. doi:10.1016/s1074-
779 7613(00)80004-7
780 Shiloh, M. U., & Nathan, C. F. (2000). Reactive nitrogen intermediates and the pathogenesis of
781 Salmonella and mycobacteria. *Curr Opin Microbiol, 3*(1), 35-42. doi:10.1016/s1369-
782 5274(99)00048-x
783 Simonet, M., Richard, S., & Berche, P. (1990). Electron microscopic evidence for in vivo
784 extracellular localization of Yersinia pseudotuberculosis harboring the pYV plasmid.
785 *Infect Immun, 58*(3), 841-845. Retrieved from
786 https://www.ncbi.nlm.nih.gov/pubmed/2307522
787 Songsungthong, W., Higgins, M. C., Rolan, H. G., Murphy, J. L., & Mecsas, J. (2010). ROS-
788 inhibitory activity of YopE is required for full virulence of Yersinia in mice. *Cell*
789 *Microbiol, 12*(7), 988-1001. doi:10.1111/j.1462-5822.2010.01448.x
790 Sugimoto, M., Sakagami, H., Yokote, Y., Onuma, H., Kaneko, M., Mori, M., . . . Tomita, M.
791 (2011). Non-targeted metabolite profiling in activated macrophage secretion.
792 *Metabolomics, 8*(4), 624-633. doi:10.1007/s11306-011-0353-9
793 Thibault, D., Jensen, P. A., Wood, S., Qabar, C., Clark, S., Shainheit, M. G., . . . van Opijnen, T.
794 (2019). Droplet Tn-Seq combines microfluidics with Tn-Seq for identifying complex
795 single-cell phenotypes. *Nat Commun, 10*(1), 5729. doi:10.1038/s41467-019-13719-9
796 Vazquez-Torres, A., Jones-Carson, J., Mastroeni, P., Ischiropoulos, H., & Fang, F. C. (2000).
797 Antimicrobial actions of the NADPH phagocyte oxidase and inducible nitric oxide
798 synthase in experimental salmonellosis. I. Effects on microbial killing by activated
799 peritoneal macrophages in vitro. *J Exp Med, 192*(2), 227-236. doi:10.1084/jem.192.2.227

800